Supporting Information

Bio-inspired Multifunctional Interface Layer for High Performance Zinc-Ion Batteries via Novel In-situ Electropolymerization

Jun Wang † [a], Xiuyang Zou† [c], Lina Song [a], Yang Hou [a,b], Jianguo Lu [d], Xiang Gao [a], Qinggang He [a], Yongyuan Ren * [a,b], Xiaoli Zhan [a,b], Qinghua Zhang * [a,b]

[a] *College of Chemical and Biological Engineering, Zhejiang University, Hangzhou 310027, China*

[b] *Institute of Zhejiang University-Quzhou, Quzhou 324000, China*

[c] *College of Chemistry, Chemical Engineering and Materials Science, Soochow University, Suzhou 215123, China*

[d] *School of Materials Science and Engineering Zhejiang University, Hangzhou 310027, China*

**Email: qhzhang@zju.edu.cn*

Y.Ren-IL@zju.edu.cn

1. Experimental Section

Materials: All chemicals were used directly without further purification. Sodium acrylate (AS, 95.0%), N, N-Methylenebisacrylamide (Bis, 99.0%), $KMnO_4$ (99.5%) and Sodium nitrate ($NaNO_3$, 99.0%) were purchased from Shanghai Aladdin Bio-Chem Technology. Ammonium persulphate (APS, 99.8%), sulfuric acid (H_2SO_4, 98.0%), $MnSO_4$ aqueous solution (0.5 M), zinc trifluoromethanesulphonate ($Zn(CF_3SO_3)_2$, 98.0%), and potassium chloride (KCl, 99.8%) were purchased from Sinopharm Chemical. Reagent Co., Ltd. Ti_3C_2 MXene powder (MX) was received from Forsman Co. Ltd., Beijing, China.

Preparation of α-MnO_2: Referring to the previous report [1], α-MnO_2 power were synthesized via the hydrothermal treatment. Concretely, 2 mL H_2SO_4 (0.5 M) and 1g $MnSO_4$ aqueous solution (0.5 M) were add into 68 mL deionized water, and the homogeneous solution was formed after magnetic stirring for 60 min. Then, 20 m L $KMnO_4$ (0.1 M) was gradually added to the above system, still keep stirring for another 60 min. Subsequently, the solution was transferred into a Teflon-lined autoclave for a hydrothermal (120 °C, 12 h). The final reaction product was collected by vacuum filtration, washed with deionized water for several times, and dried in vacuum at 60 °C overnight.

Preparation of PAAS@Zn and MX/PAAS@Zn : The in-situ electropolymerization was carried out on the electrochemical workstation (CHI660E, ChenHua). 0.33 g AS (monomer), 0.12 g APS (initiator), 0.054 g Bis (crosslinking agent) and 0.85 g $NaNO_3$

(catalyst) was dissolved in 50 mL of 1 M KCl. Under three-electrode system, the Zn electrode was acted as working electrode, Pt electrode was the opposite and reference electrode. Set the reduction voltage to -0.7 V and pulsed cycle 100 times to fabricate the PAAS@Zn anode. Then soaked in deionized water for 6 h to remove residual KCl solution on the surface and drying at 60 °C for 3h. To be stressed, under appropriately negative potential, the persulfate anions was reduced to free radicals, polymerization reaction was initiated, and simultaneous gel layer was anchored on the surface of the electrode. Similarly, MX/PAAS@Zn was prepared by adding 20 mg of MXene on the basis of the above solution for PAAS@Zn.

Preparation of electrolyte: Here, 2M $Zn(CF_3SO_3)_2$ electrolyte was prepared by dissolving a certain amount of $Zn(CF_3SO_3)_2$ in deionized (DI) water to acquire homogeneous solution. For Zn/ MnO_2 batteries, the electrolyte was 2M $Zn(CF_3SO_3)_2$ + 0.1M $MnSO_4$.

Preparation of electrodes: The purchased Zn foil (99.99%) was polished with sandpaper and punched into a disc to be employed as Zn anode. Similarly, the MX/PAAS@Zn and PAAS@Zn anodes were created by cutting the MX/PAAS@Zn and PAAS@Zn foils into discs, respectively. Herein, all the anodes were uniform in size of 14 mm. The MnO_2 cathode was obtained through mixing 70 wt% MnO_2 powders, 20 wt% conductive carbon, and 10 wt% poly vinylidene fluoride (PVDF) in N-methyl-2-pyrrolidone (NMP) solution. Then, the obtained slurry was coated on the Ti foil and dried at 80 °C for 24 h under vacuum. Then, cut into 12 diameter discs for next use and the mass loading of active material was about 1.0-1.4 mg cm^{-2}.

Materials Characterizations: X-ray diffraction (XRD, Bruker D2-Phaser) was used to test the crystal structure of the materials with Cu Kα radiation from 5° to 90°. The morphology characterization of the materials was conducted via fieldemission scanning electron microscopy (FESEM; ZEISS, Germany) equipped with energy-dispersive X-ray spectroscopy (EDS) mapping. The X-ray photo electron spectroscopy (XPS, PHOIBOS150, Germany) was employed to characterize the surface evolution of Zn anode. Surface roughness before and after cycle of the Zn anode were obtained by 3D optical surface profiler (NewView 9000, ZYGO Corp., USA).

Assembly of symmetric cells and Zn/MnO_2 full cells: Standard CR2032-type coin cells were assembled for electrochemical performance assessment. The symmetric and asymmetrical cells were assembled into CR2032 coin-type cells with zinc anodes (bare Zn, PAAS@Zn or MX/PAAS@Zn), glass fiber separator (Whatman, GF/D), Zn or Cu electrode and 2M $Zn(CF_3SO_3)_2$ aqueous electrolyte. Full cells of Zn-MnO_2 were assembled by MnO_2 powder as the cathode material, bare Zn, PAAS@Zn or MX/PAAS@Zn as the anode, 2M $Zn(CF_3SO_3)_2$ as the electrolyte, respectively.

Electrochemical Measurements: The electrochemical workstation (CHI660E, Shanghai ChenHua, Instruments Co.) was employed to measure cyclic voltammetry (CV), electrochemical impedance spectroscopy (EIS) and Chronoamperometry (CA) test. The three-electrode system was implemented to obtain Tafel and linear sweep voltammetry (LSV) curves with the Zn plate (PAAS@Zn or MX/PAAS@Zn), platinum plate, and standard hydrogen electrode (SHE) as working, counter, and reference

electrode, respectively. All the cycling tests were performed on NEWARE CT-4008 battery testing system.

Measurements of Zn^{2+} transference number: To contrast the kinetics, the transference number of Zn^{2+} ($t_{Zn^{2+}}$) was regarded as an important performance parameter, which could evaluate by the following equation:

$$t_{Zn^{2+}} = \frac{Is(\Delta V - I0R0)}{Is(\Delta V - IsRs)}$$

where ΔV is the constant polarization voltage applied (25 mV), I_0 and I_s are the initial and steady-state current, while R_0 and R_s are the initial and steady-state resistance, respectively.

Measurements of Zn^{2+} deposition/dissolution activity: Zn deposition depends on whether the desolvation process is unhindered. The activation energy (Ea) can evaluate by Arrhenius equation, which is analyzed from EIS of symmetrical cells at different temperatures. Shown as the following equation:

$$\frac{1}{R_{ct}} = A\exp\left(\frac{-Ea}{RT}\right)$$

where R_{ct} is the charge-transfer resistance, A is the frequency factor, R is the gas constant, and T is the absolute temperature, respectively.

2. Calculation method:

The Density Functional Theory (DFT) calculation were conducted in CASTcEP program.[2,3] The structure optimization was performed at general gradient approximation with Perdew-Burke-Ernzerhof (GGA-PBE) exchange-correlation functional level to determine their stable

locations using a 4 × 4 × 2 supercell model. The generalized gradient approximation method proposed by Perdew et al. with van der Waals correction proposed by Grimme (DFT-D3) is chosen because of its suitable description of long-range vdW interactions [4,5] The C axis was set as 20 Å to ensure enough vacuum to avoid interactions between two periods. Spin-polarized calculations were employed with the double numerical polarization basis set. The Energy cutoff was set to 489.9 eV and k-point set was 1 × 1 × 1. The SCF convergence for each electronic energy was set as 2.0 × 10^{-6} eV/atom and the Max. SCF cycles was set 100. The binding energies were calculated by following equation:[6]

$$\Delta E_{bind}=E_{total} - E_{Zn} - E_{PAAS}$$

The E_{total} represents the total energy of PAAS and Zn^{2+}, E_{Zn} is the total energy of Zn^{2+}, and E_{PAAS} is the total energy of PAAS, respectively.

The hydrogen adsorption energy is defined as:

$$\Delta E_H = E_{(substrate+H)} - E_{substrate} - 1/2\ E_{H2}$$

where $E_{(substrate+H)}$ is the energy of the substrate with a H atom adsorbed, $E_{substrate}$ is that of the substrate without adsorbed H, and E_{H2} is that of gas phase H_2 molecule.

The hydrogen adsorption free energy ΔG_H was defined as:

$$\Delta G_H = \Delta E_H + \Delta E_{ZPE} - T\Delta S_H$$

Where ΔE_H is the hydrogen adsorption energy, ΔE_{ZPE} is the zero-point energy difference, T is the temperature, and ΔS_H is the entropy difference for hydrogen between the adsorbed state

and the gas phase. The entropy of hydrogen adsorption is calculated as $\Delta S_H = 1/2 S_{H2}$, where S_{H2} is the entropy of hydrogen molecule inthe gas phase at standard conditions.

6. Experimental data

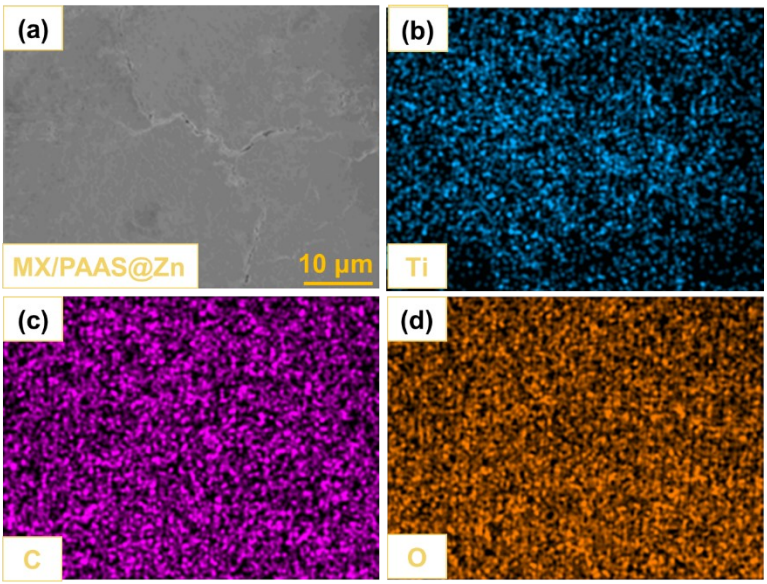

Figure.S1 SEM-mapping results of MX/PAAS@Zn anode

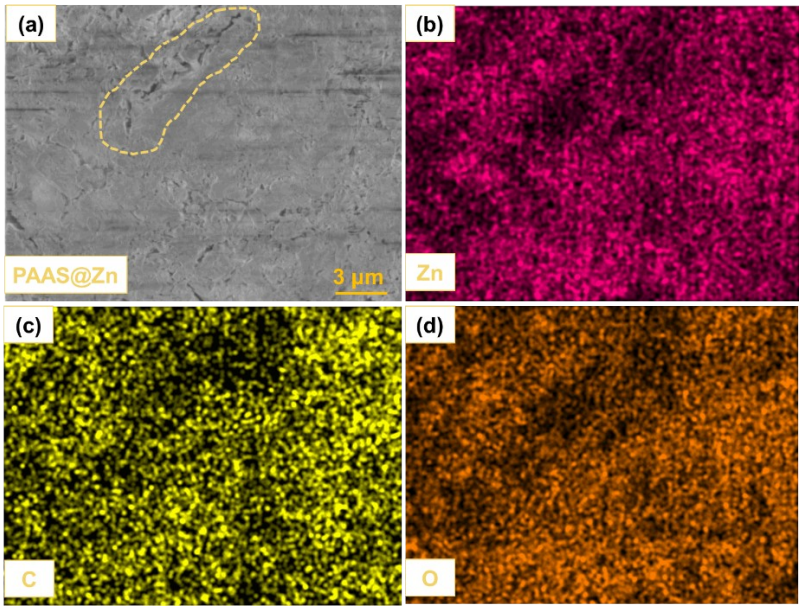

Figure.S2 SEM-mapping results of PAAS@Zn anode

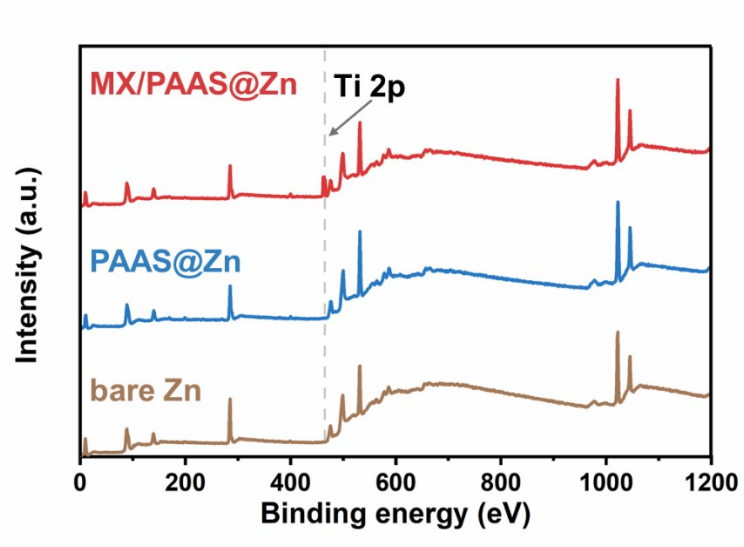

Figure.S3 XPS survey of bare Zn, PAAS@Zn and MX/PAAS@Zn

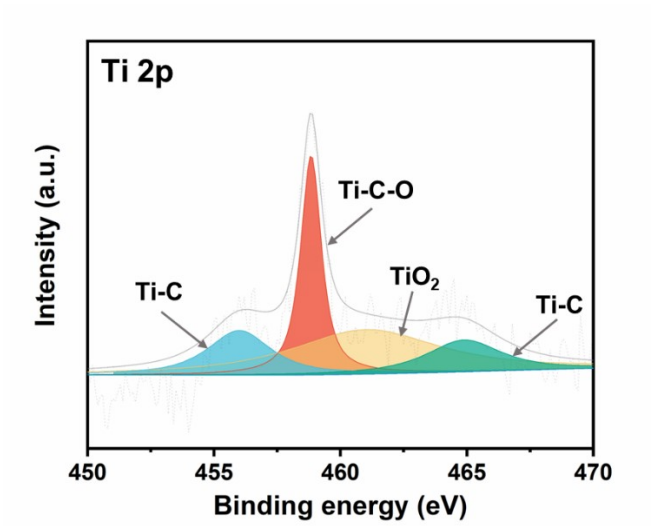

Figure.S4 High-resolution XPS spectrum of Ti 2p of MX/PAAS@Zn

Table.S1 High-resolution XPS spectrum of various anodes

Binding energy (eV)	Zn $2p_{3/2}$		Zn-O		Zn $2p_{1/2}$
MX/PAAS@Zn	1021.8		1022.6		1045.3
PAAS@Zn	1021.7		1022.4		1045.2
bare Zn	1021.4				1044.6
Binding energy (eV)	**Ti-C**	**C-C**	**C=C**	**C-O**	**O-C=O**
MX/PAAS@Zn	283.7	284.5	285.0	285.8	288.5
PAAS@Zn		284.3	285.0	285.5	288.4
bare Zn		284.2		285.7	
Binding energy (eV)	**Ti-O**		**C-O**		**C=O**
MX/PAAS@Zn	531.0		531.8		532.4
PAAS@Zn			531.4		532.2
bare Zn	529.7 (Lattice oxygen)		531.3 (Absorbed oxygen)		

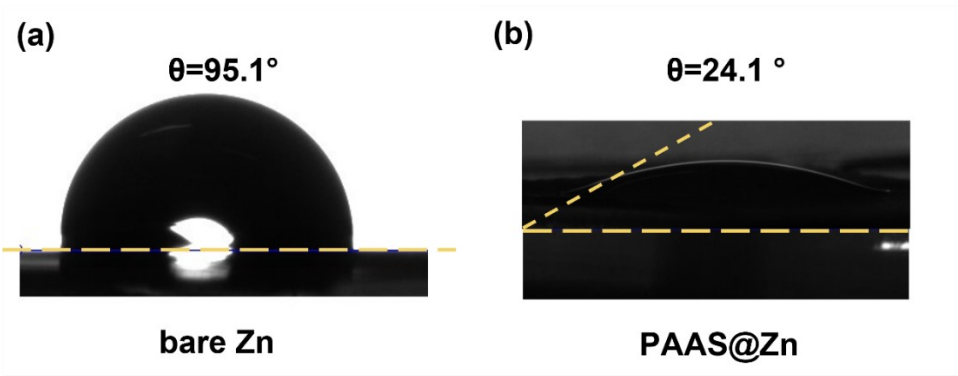

Fig.S5 Contact angle of electrode and electrolyte (2M $Zn(CF_3SO_3)_2$). (a) Bare Zn, (b)PAAS@Zn anode

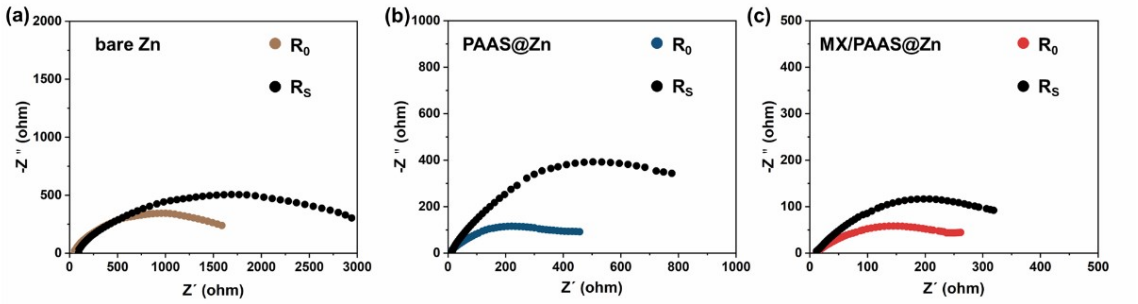

Figure. S6 The A. C. impedance results of the all the electrodes before and after CA measurement (200 mV). (a) bare Zn, (b) PAAS@Zn and (c) MX/PAAS@Zn

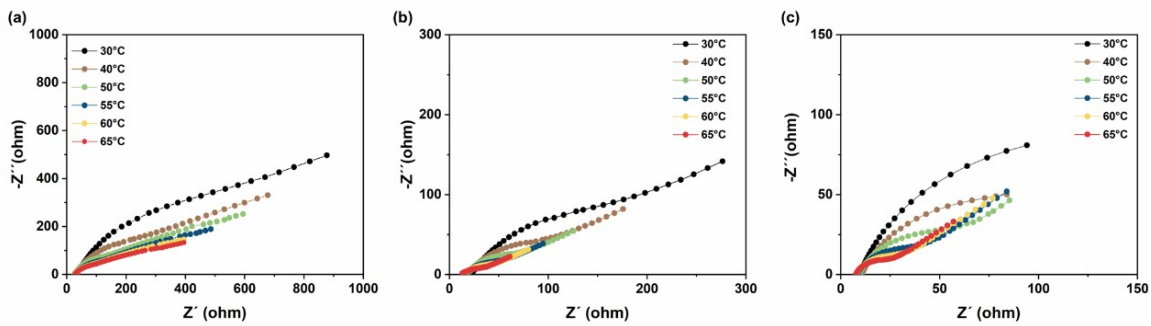

Figure. S7 Nyquist plots of the at different temperatures for symmetric cells based on (a) bare Zn, (b) PAAS@Zn and (c) MX/PAAS@Zn electrodes

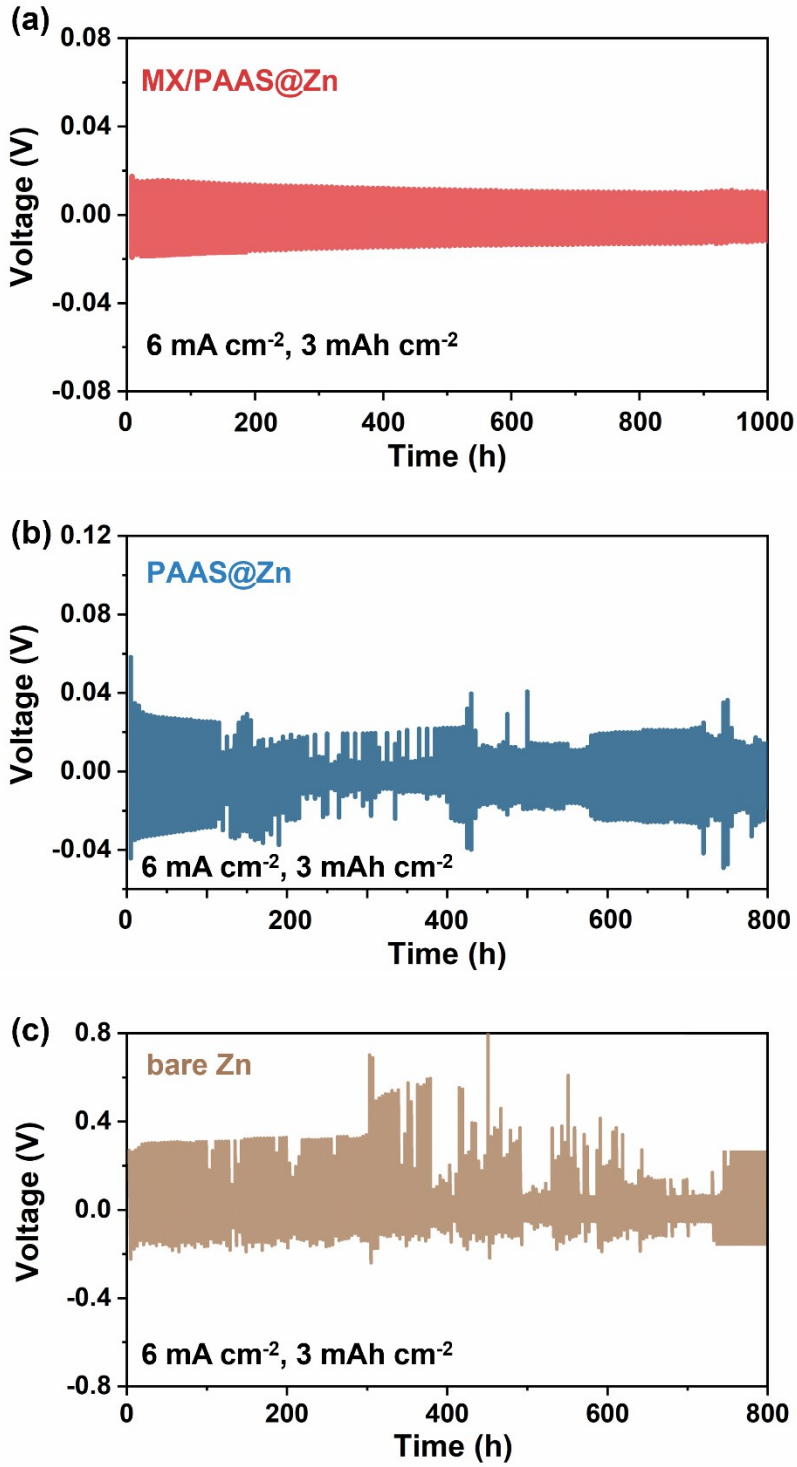

Figure. S8 Long-term cycling performance of (a) MX/PAAS@Zn, (b) PAAS@Zn and (c) bare Zn symmetric cells at the current density of 6 mA cm^{-2} for 0.5 h per cycle

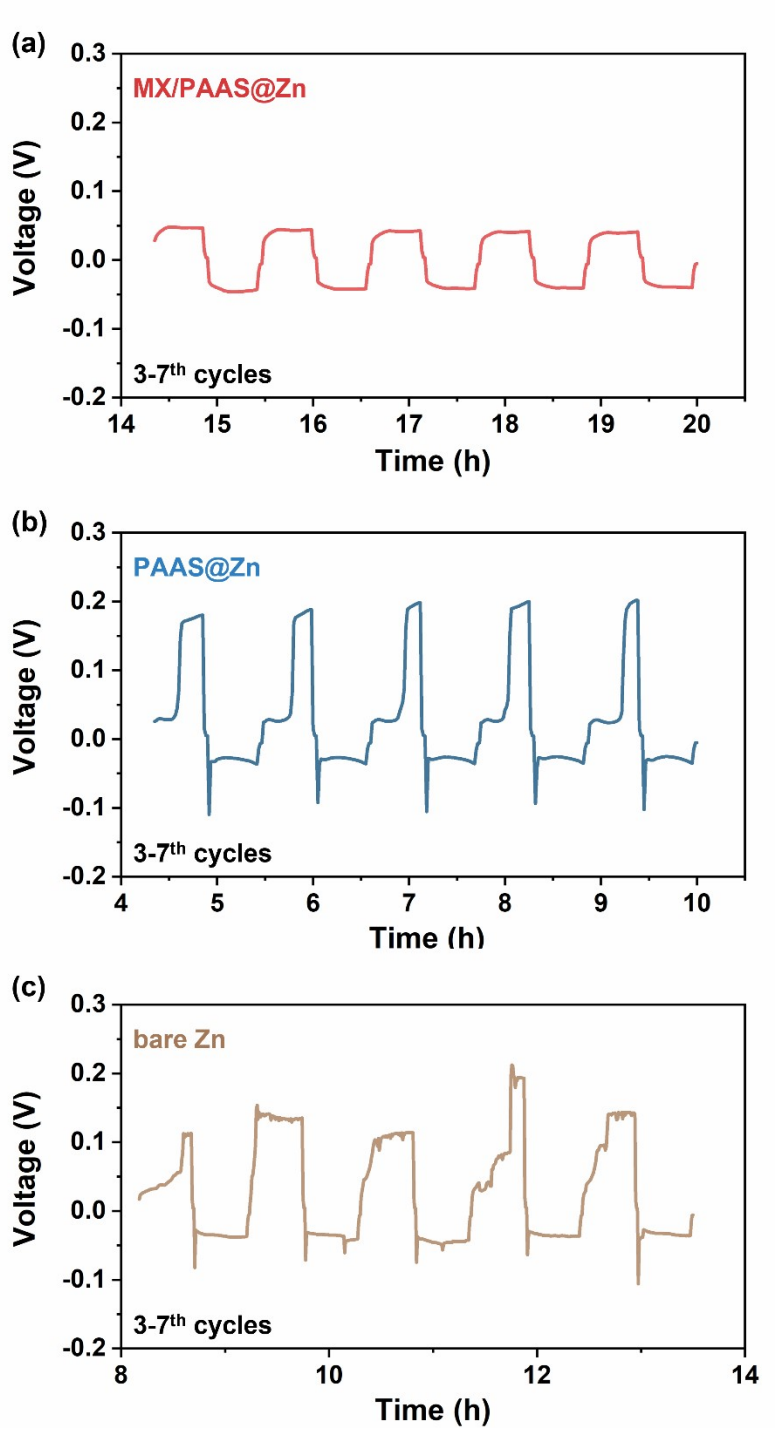

Figure. S9 The voltage profiles of symmetric cell for (a) MX/PAAS@Zn, (b) PAAS@Zn and (c) bare Zn at the current density of 10 mA cm^{-2} for 0.5 h per cycle (3-7th cycles)

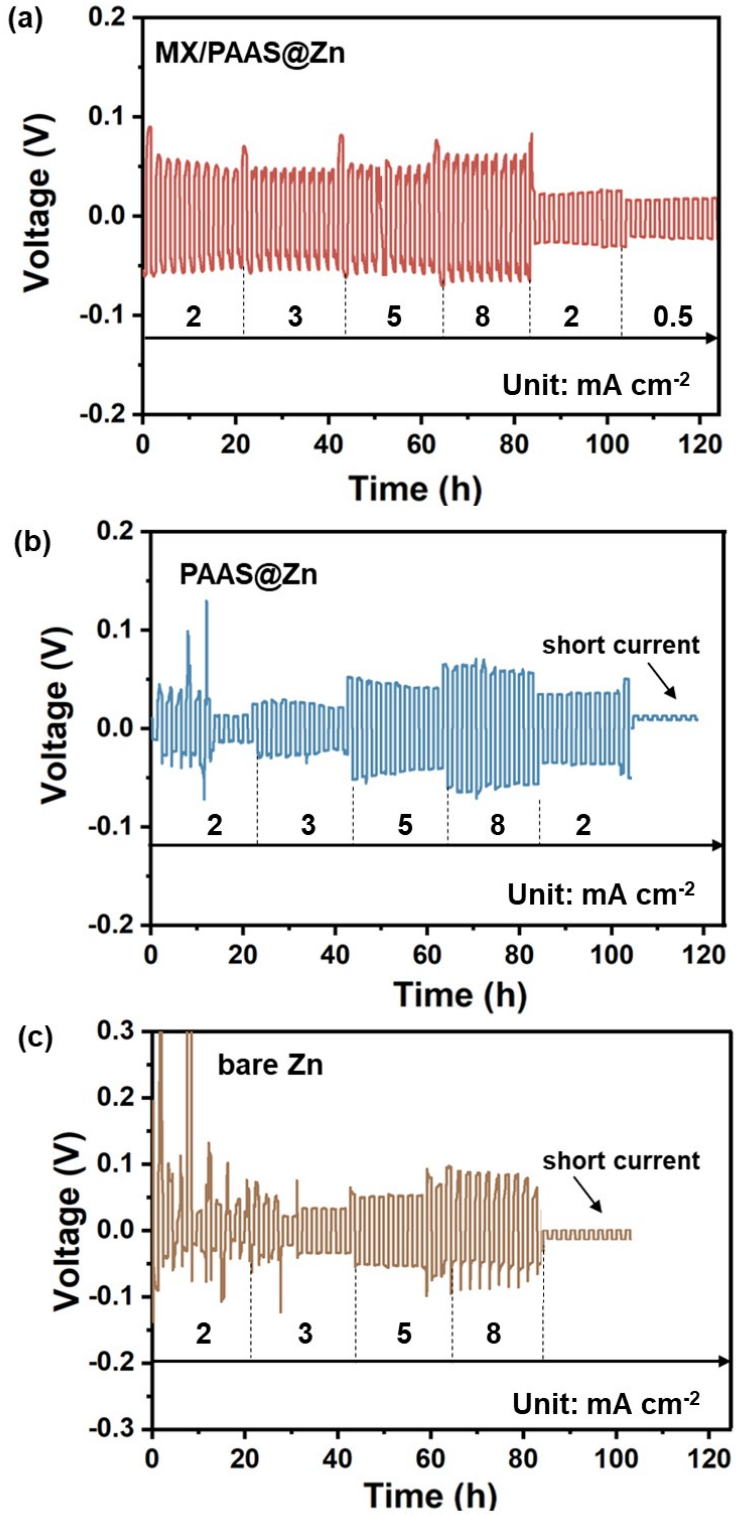

Figure. S10. Rate performance of (a) MX/PAAS@Zn, (b) PAAS@Zn and (c) bare Zn symmetric cells

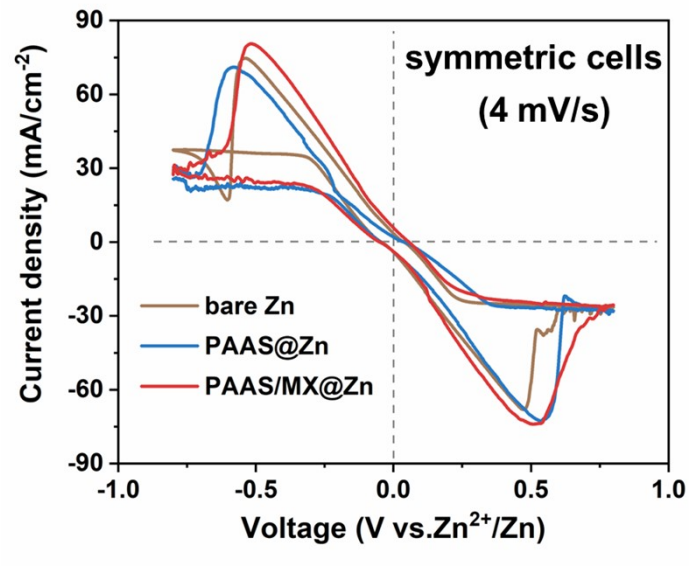

Figure. S11 Cyclic voltammetry curves of symmetric cells at 4 mV/s

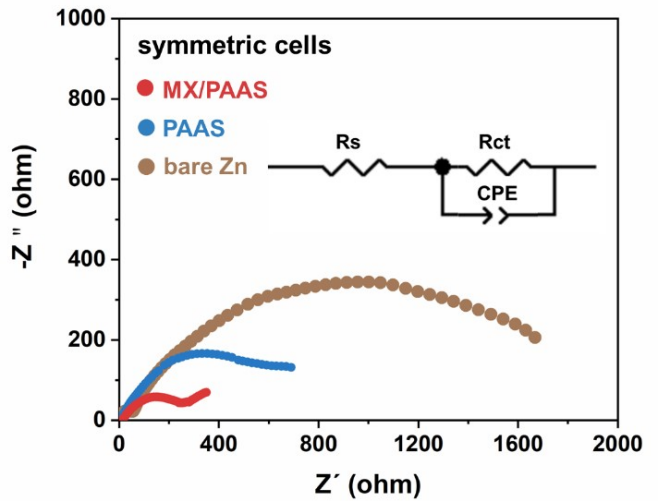

Figure. S12 Nyquist plots of fresh symmetric cells

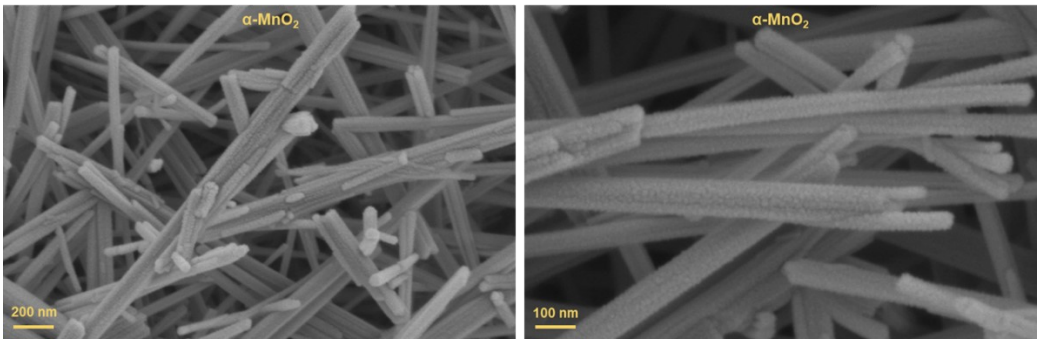

Figure. S13 SEM results of α-MnO_2

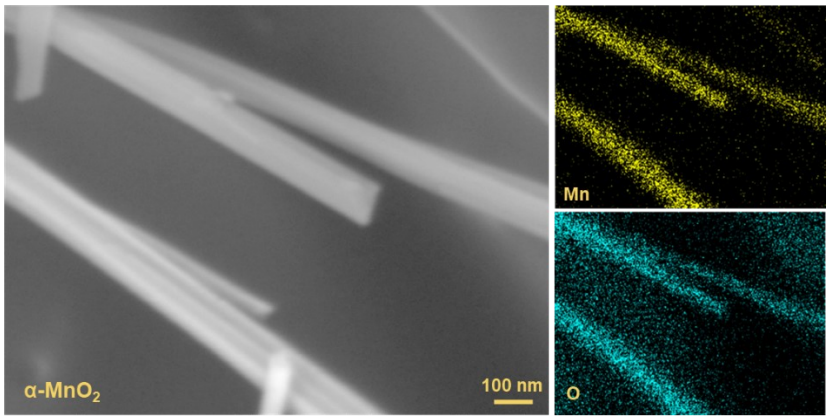

Figure. S14 EDS results of α-MnO_2

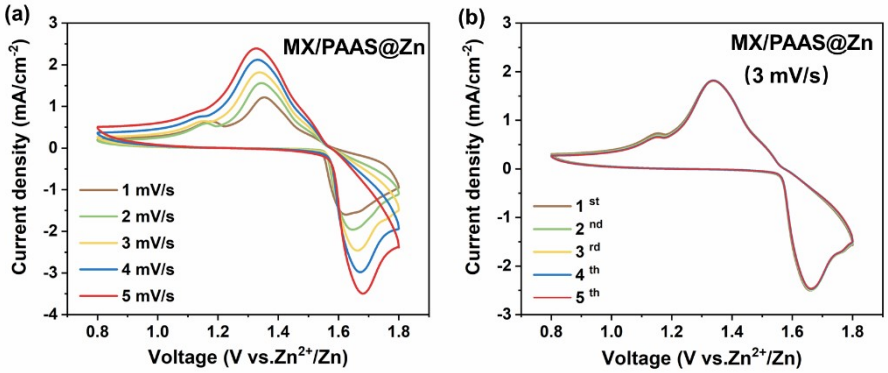

Figure. S15 Cyclic voltammetry curves of MnO_2 || MX/PAAS@Zn batteries. (a) different scan rate (1-5 mV/s) and the first five cycles at 3 mV/s

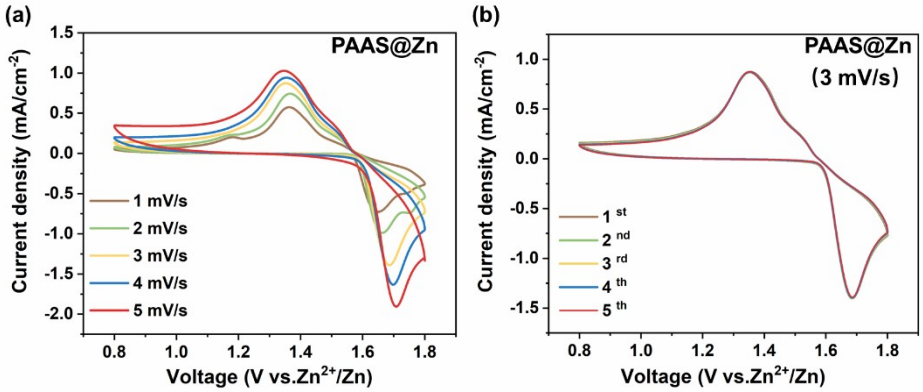

Figure. S16 Figure. S8 Cyclic voltammetry curves of MnO_2 || PAAS@Zn batteries. (a) different scan rate (1-5 mV/s) and the first five cycles at 3 mV/s

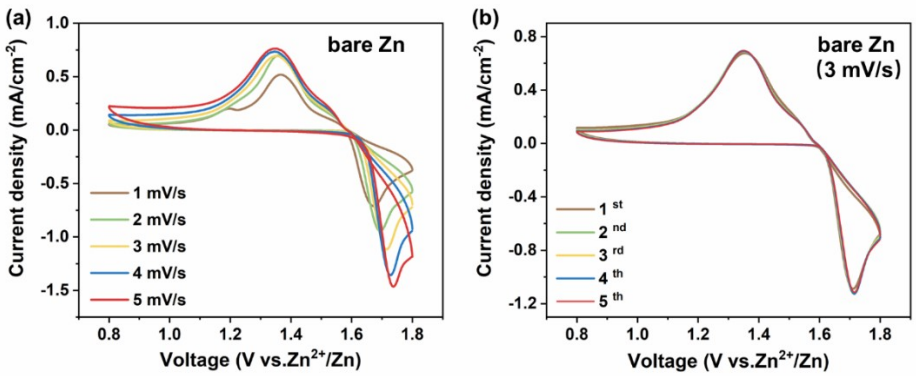

Figure. S17 Cyclic voltammetry curves of MnO_2||bare Zn batteries. (a) different scan rate (1-5 mV/s) and the first five cycles at 3 mV/s

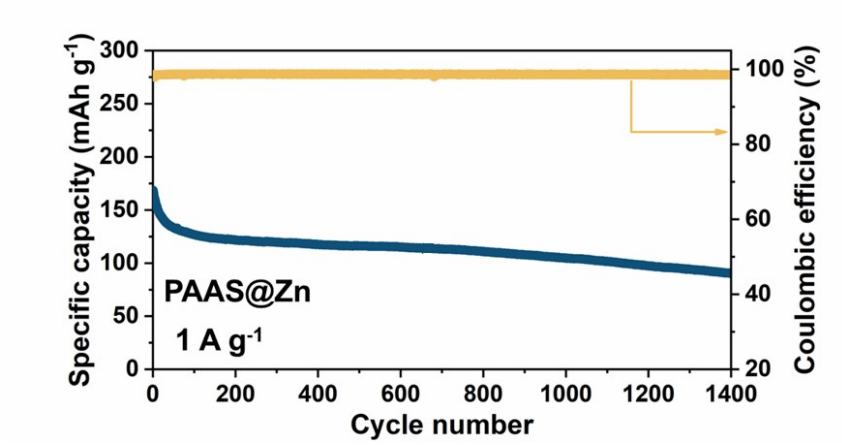

Figure. S18 Long-term cycling performances of MnO_2||PAAS full cells

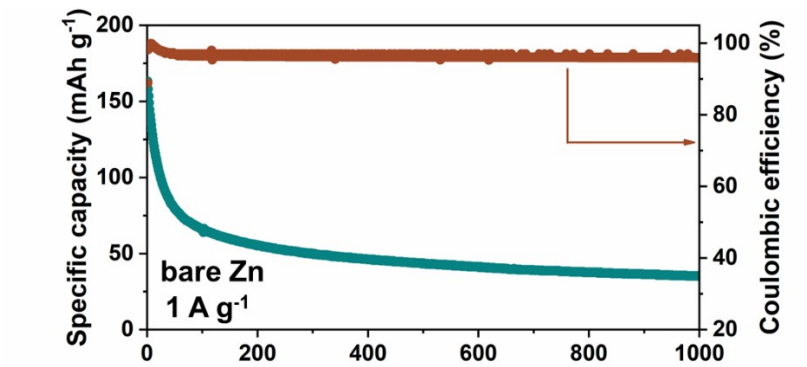

Figure. S19 Long-term cycling performances of MnO_2||bare Zn full cells

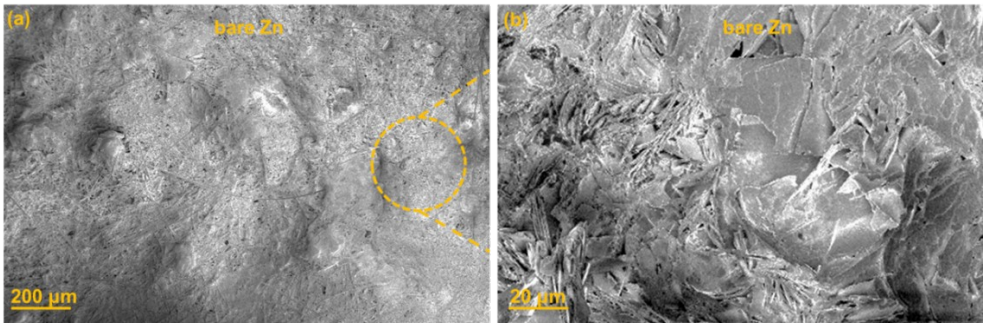

Figure. S20 SEM image of bare Zn anode after 1000 plating/stripping cycles at 6 mA cm^{-2}, 3 mAh cm^{-2}

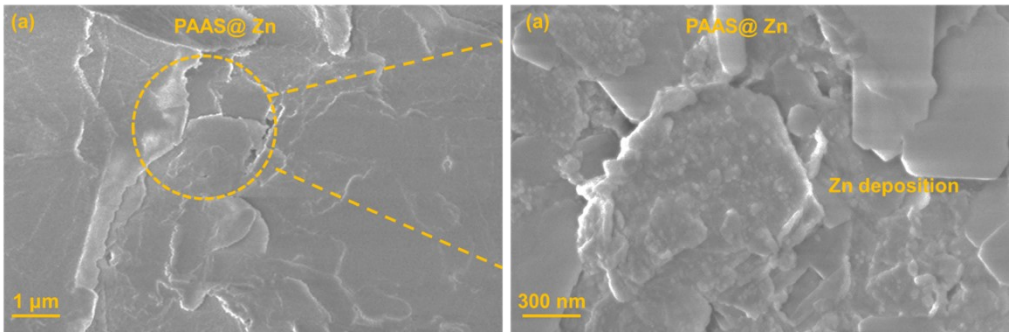

Figure. S21 SEM image of PAAS@Zn anode after 1000 plating/stripping cycles at 6 mA cm^{-2}, 3 mAh cm^{-2}

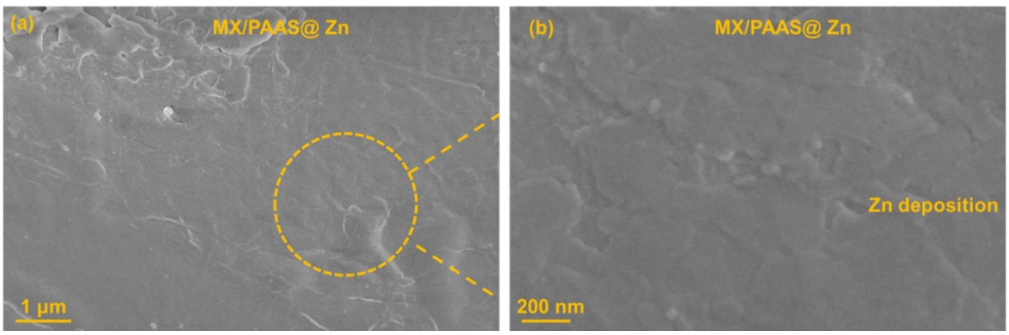

Figure. S22 SEM image of MX/PAAS@Zn anode after 1000 plating/stripping cycles at 6 mA cm^{-2}, 3 mAh cm^{-2}

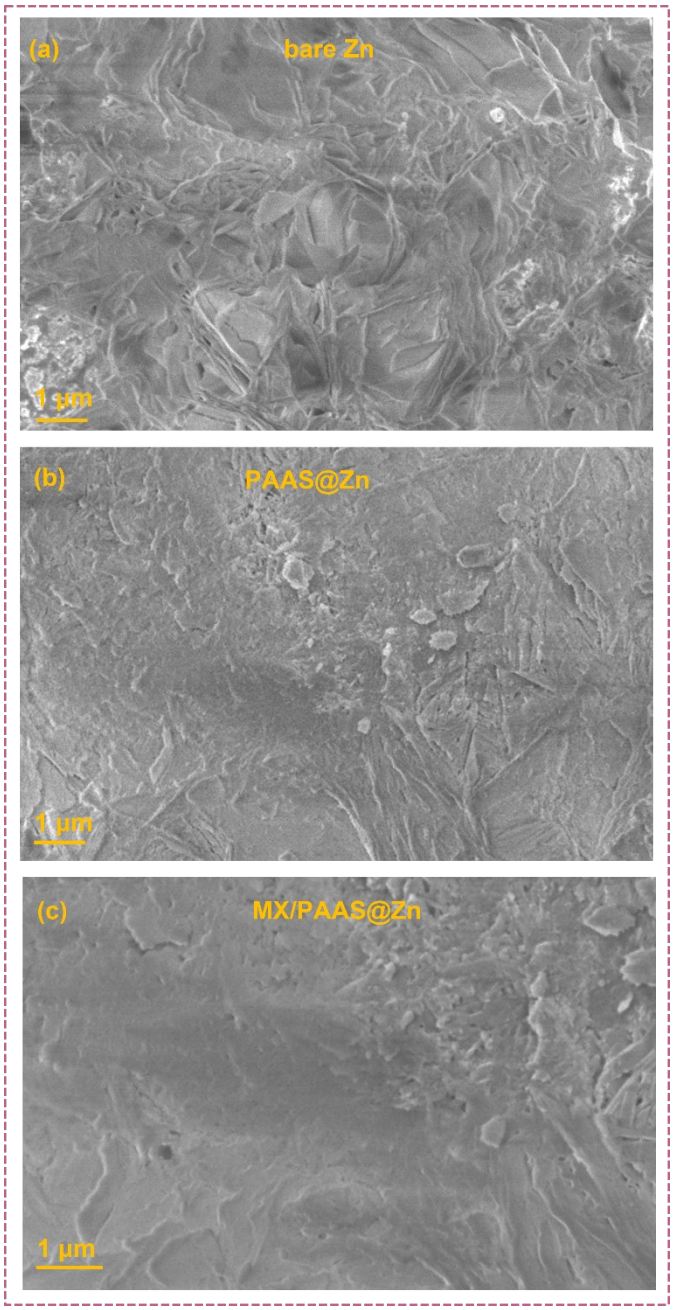

Figure. S23 SEM image of (a) bare Zn (b) PAAS@Zn and (c) MX/PAAS@Zn anodes after 500 plating/stripping cycling at 10 mA cm^{-2}, 10 mAh cm^{-2}

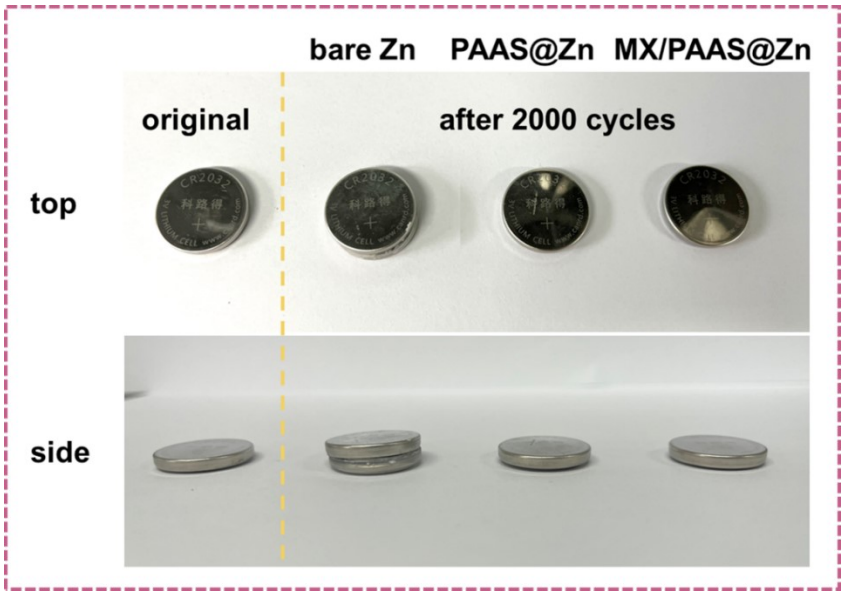

Figure. S24 Volume expansion comparison of bare Zn, PAAS@Zn and MX/PAAS@Zn symmetric batteries after 2000 plating/stripping cycling.

Figure. S25 The corresponding optical images of each component for bare Zn, PAAS@Zn and MX/PAAS@Zn symmetric batteries after 2000 plating/stripping cycling

Tabel. S2 The mechanical property of PAAS and MX/PAAS interface layers via in-situ electropolymerization

Sample	Ultimate stress (%)	Young modulus (kPa)	Toughness (kJ m^{-3})	Fracture energy (J m^{-2})
PAAS	247	720	152	76
MX/PAAS	320	4355	6835	9884

References

[1] H. Pan, Y. Shao, P. Yan, Y. Cheng, K. S. Han, Z. Nie, C. Wang, J. Yang, X. Li, P. Bhattacharya, K. T. Mueller, J. Liu, *Nat. Energy* **2016**, *1*, 16039.

[2] F. Xing, Y. Nakaya, S. Yasumura, K. Shimizu, S. Furukawa, *Nat. Catal.* **2022**, *5*, 55.

[3] F. Wang, O. Borodin, T. Gao, X. Fan, W. Sun, F. Han, A. Faraone, J. A. Dura, K. Xu, C. Wang, *Nat. Mater.* **2018**, *17*, 543.

[4] J. P. Perdew, K. Burke, M. Ernzerhof, Phys Rev Lett **1996**, *77*, 3865-3868.

[5] L. Goerigk, A. Hansen, C. Bauer, S. Ehrlich, A. Najibi, S. Grimme, *Phys Chem Chem Phys.* **2017**, *19*, 32184-32215.

[6] W. Gao, Y. Chen, B. Li, S. Liu, Q. Jiang, *Nat. Catal.* **2020***, 11*, 96.